PRAMANA — journal of physics

Vol. 82, No. 3
March 2014
pp. 529–536

Step index fibre using laser interferometer

A M HAMED
Physics Department, Faculty of Science, Ain Shams University, Cairo 11566, Egypt
E-mail: amhamed73@hotmail.com

MS received 10 May 2013; revised 17 August 2013; accepted 25 November 2013
DOI: 10.1007/s12043-014-0706-9; ***e*Publication:** 4 March 2014

Abstract. A model is suggested to describe the fringe shift which occurs due to the phase variations of cladded glass fibre introduced between the two plates of the liquid wedge interferometer illuminated with a He–Ne laser. The fringe shift of the phase object which appears in the denominator of the Airy distribution formula of the multiple beam interference is represented in the harmonic term. An experiment is conducted using liquid wedge interferometer where the step index glass fibre of a nearly quadratic thickness variation is introduced between the two plates of the interferometer. The obtained fringe shift shows a good agreement with the proposed quadratic model. The Matlab code is written to plot the interferometer fringes comprising the shift of the step index fibre. Secondly, recognition of elliptical fibres is outlined using tomographic imaging. Finally, results and concluding remarks are given.

Keywords. Multiple beam interference; laser radiation; tomographic images; step index and graded index fibres.

PACS Nos 42; 02; 06

1. Introduction

Tolansky [1] has obtained an approximate formula of Airy summation and pointed out the main features between the beams forming multiple-beam fringes at infinity by using a plane parallel plate and those forming multiple beam localized fringes. In the case of the wedge, the successively multiply reflected beams are not in phase in exact arithmetic series while in the case of plane parallel plates the path difference between any two successive beams is $\lambda/2$. The optimum condition for producing multiple beam localized fringes, reached by Tolansky, necessitates small interferometer wedge angle α in order to fulfill the Airy's summation conditions. Barakat and Mokhtar [2] found that the permitted limit is $(3/8)\lambda$. In other studies [3–10], interference was obtained using synthetic optical fibres. They considered ray optics approximation using monochromatic light emitted from mercury and other spectral lamps. Also, Barakat has obtained the right formula, which is based on ray optics, of multiple beam fringes crossing a fibre of circular transverse cross-section immersed in a silvered liquid wedge. His work was followed by others [8]

who extended the analysis to multilayer fibres. Hamza *et al* [9] determined the refractive indices and birefringence of fibres having irregular transverse sections of homogeneous fibres. Boggs *et al* [11] and Presby *et al* [12] described automated transverse interferometer method and described the index profile of graded index fibre. Recently, Hamed [13] has considered the effect of the wedge angle α on the arithmetic series using a Gaussian laser illumination. The modified Airy distribution is obtained using Fourier imaging applied on fibres. The effect of laser modulation on the contrast and sharpness of fringes has been investigated. Then, the fringe shift of unclad fibres is experimentally obtained and a model is constructed to describe this single shift [14].

The radon function computes projections of an image matrix along specified directions. A projection of a two-dimensional function $f(x, y)$ is a set of line integrals. The radon function computes the line integrals from multiple sources along parallel paths, or beams, in a certain direction. The beams are spaced 1 pixel unit apart. To represent an image, the radon function takes multiple, parallel-beam projections of the image from different angles by rotating the source around the centre of the image [15–19]. Three-dimensional (3D) imaging by holographic tomography can be performed for a fixed detector through rotation of either the object or the illumination beam [20].

In this study, we suggest a model of two step variations to describe the thickness distribution of the step index fibres having circular transverse cross-sections. The Airy distribution is written in the case of fibre modulation giving nearly quadratic shift variations inside the core.

An experiment [5] is done using liquid wedge interferometer where a step index fibre is enclosed between the two plates of the interferometer. The interferometer is illuminated by a He–Ne laser. The quadratic theoretical model is compared with the experimental shift of the fibre which shows good agreement. In the following section, theoretical analysis is presented including the quadratic model for the fringe shift. Finally, results and discussion are given.

2. Theoretical analysis

2.1 *Modelling of the fringe shift in cladded fibres*

We propose the following model to describe the cladded fibre placed inside a liquid wedge interferometer. For simplicity, we assume square interferometer plates of dimensions $2a$, $2b$ and refractive index μ_{L}. The fibre radius is r_{f} and the core radius is r_{c} with skin and core indices μ_{s}, μ_{c} respectively.

Hence, the object immersed in the liquid is analytically represented as follows:

$$G(x, y) = g_{\mathrm{c}}(x, y) + g_{\mathrm{s}}(x, y) + g_{\mathrm{L}}(x, y), \tag{1}$$

where $g_{\mathrm{c}}(x, y) = 1$; for $x^2 + y^2 < r_{\mathrm{c}}^2$ for the core central region, $g_{\mathrm{s}}(x, y) = 1$; for $r_{\mathrm{c}}^2 < x^2 + y^2 < r_{\mathrm{f}}^2$ for the skin region of the fibre and $g_{\mathrm{L}}(x, y) = 1$; for $x < (a - r_{\mathrm{f}})$ and $y < (b - r_{\mathrm{f}})$ with $a = b$ for square liquid wedge.

For uniform illumination emitted from spatially filtered laser beam, the Fourier spectrum of the object information is calculated operating the FT upon eq. (1) to get

$$\tilde{g}(u, v) = \frac{2J_1(w_1)}{w_1} + \left[\frac{2J_1(w_2)}{w_2} - \frac{2J_1(w_1)}{w_1}\right] + \frac{\sin(u)}{u}\frac{\sin(v)}{v}, \tag{2}$$

where $\rho = (u, v)$ is the radial coordinate in the Fourier plane and $r = (x, y)$ is the radial coordinate in the object plane. The reduced coordinates w_1 and w_2 are given by

$$w_1 = 2\pi r_c \rho/\lambda f \quad \text{and} \quad w_2 = 2\pi r_f \rho/\lambda f.$$

A quadratic model is assumed for the fringe shift of step index fibre. It is mathematically represented as follows:

$$\begin{aligned} t_p(y) &= t_0\left[\left(\frac{y_1}{r_f}\right)^2 + \left(\frac{y_2}{r_f}\right)^2\right]; \ 0 < y_1 < r_c \text{ and } r_c < y_2 < r_f \\ &= t; \qquad\qquad\qquad\qquad\qquad\qquad y > y_1 + y_2 \end{aligned}. \tag{3}$$

Equation (3) represents a model which assumes a quadratic dependence that will describe the necessary features of the core and skin layers.

In eq. (3), t_0 is the maximum shift inside the fibre. The fringe phase shift in a liquid wedge interferometer provided with step index fibre is described by eqs (4) and (5):

The phase of the step index fibre is calculated as follows:

$$\phi(y) = \left(\frac{2\pi}{\lambda}\right)\left[2\mu_L t + 4(\mu_c - \mu_L)\, t_0\left(\frac{y_1}{r_f}\right)^2 + 4(\mu_s - \mu_L)\, t_0\left(\frac{y_2}{r_f}\right)^2\right]. \tag{4}$$

Since $t = z\tan\alpha$ for the wedge interferometer of wedge angle (α), then eq. (4) becomes

$$\begin{aligned} \phi(y) = \left(\frac{2\pi}{\lambda}\right)\Bigg[&2\mu_L z\tan(\alpha) + 4(\mu_c - \mu_L)\, t_0\left(\frac{y_1}{r_f}\right)^2 \\ &+ 4(\mu_s - \mu_L)\, t_0\left(\frac{y_2}{r_f}\right)^2\Bigg]. \end{aligned} \tag{5}$$

The interfringe spacing of the straight line fringes is given by $\Delta z = \lambda/2$.

2.2 *Tomographic imaging of different cross-sections of fibres*

The circular cross-section of the unclad fibre is defined in the (x, y) plane as follows:

$$P(x, y) = 1; \quad |r/r_f| \le 1. \tag{6}$$

In eq. (1), r_f is the radius of the fibre.

Assuming Gauss illumination coming from the laser beam, the whole tomography pattern is built by scanning the object at different angles from 0° to 180°.

The recorded image at certain angle θ, is given as follows:

$$\begin{aligned} R_\theta\left(x'\right)_{\text{Gauss}} = &\int_{-\infty}^{\infty} \exp\left[\frac{-\left(x'^2 + y'^2\right)}{w_0^2}\right] \\ &\times P\left(x'\cos\theta - y'\sin\theta\,,\ x'\sin\theta + y'\cos\theta\right) \mathrm{d}y'. \end{aligned} \tag{7}$$

Since there is a radial symmetry of revolution for the circular cross-section of the fibre, $r(x, y) = r(x', y')$ and w_0 is the waist of the laser beam.

For coherent uniform illumination incident upon the aperture the complex amplitude of tomography pattern is computed from eq. (6), setting the Gauss pupil equal to unity for uniform illumination, as follows:

$$R_\theta(x')_{\text{uniform}} = \int_{-\infty}^{\infty} P(x'\cos\theta - y'\sin\theta, x'\sin\theta + y'\cos\theta)\mathrm{d}y'. \tag{8}$$

The point spread function (PSF) of the imaging system, using Gauss illumination, is computed by operating the Fourier transform upon the multiplication product of the fibre cross-section and the illumination Gauss function as follows:

$$\begin{aligned}\text{PSF} &= \text{FT}\left\{\exp\left[\frac{-\left(x^2+y^2\right)}{w_0^2}\right]P(x,y)\right\}\\ &= \exp\left[-w_0^2\left(u^2+v^2\right)\right] \otimes 2J_1\left(u^2+v^2\right)/\left(u^2+v^2\right).\end{aligned} \tag{9}$$

The symbol $\otimes$ in eq. (4) is used for convolution operation. Hence, the PSF of the imaging system is computed from the convolution product of the Fourier transform of each function as shown in eq. (10).

$$\text{FT}\left[\frac{-\left(x^2+y^2\right)}{w_0^2}\right] = \exp\left[-w_0^2\left(u^2+v^2\right)\right]$$

and

$$\text{FT}\left[P_1(x,y)\right] = \frac{2J_1\alpha\left(u^2+v^2\right)^{1/2}}{\left(u^2+v^2\right)^{1/2}\alpha}; \quad \alpha = \frac{2\pi r_\text{f}}{\lambda f}. \tag{10}$$

The point spread function (PSF) is computed numerically by taking the Fourier transform of the fibre cross-section.

In the case of step index fibre, the PSF of the circular cross-section is computed as follows:

$$\text{FT}\left[P_2(x,y)\right] = \frac{2J_1\alpha_1\left(u^2+v^2\right)^{1/2}}{\left(u^2+v^2\right)^{1/2}\alpha_1} - \frac{2J_1\alpha_2\left(u^2+v^2\right)^{1/2}}{\left(u^2+v^2\right)^{1/2}\alpha_2}; \tag{11}$$

$$\alpha_1 = 2\pi r_\text{f}/\lambda f \quad \text{and} \quad \alpha_2 = 2\pi r_\text{c}/\lambda f.$$

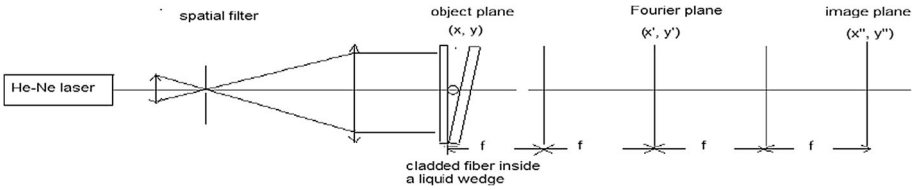

Figure 1. Optical system used to record the modulated multiple beam interference using cladded fibre as an object. The liquid wedge interferometer has a refractive index of 1.516 while the fibre refractive index is 1.5154 for the core and 1.5161 for the skin.

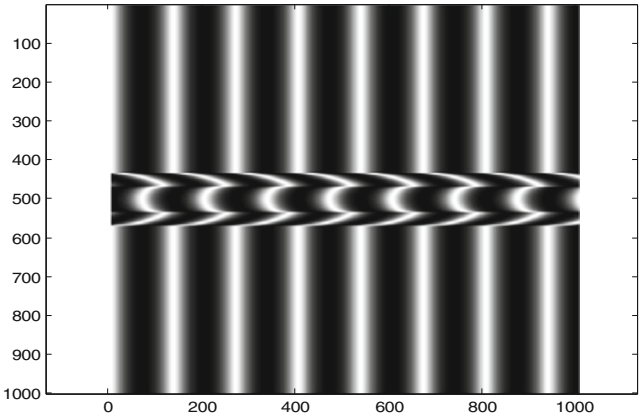

Figure 2. Theoretical imaging of multiple beam interference modulated by step index fibre of fibre radius equal to two times the core radius. The image has matrix dimensions 1024 × 1024 pixels. The fibre diameter has 128 pixels while the core diameter has 64 pixels.

3. Results and discussion

The optical system used to record multiple beam interference modulated by a cladded glass fibre is shown in figure 1. The system is illuminated by a He–Ne laser at $\lambda = 633$ nm, and is spatially filtered before incident upon the interferometer jig. The interference is imaged using optical microscope.

The liquid wedge interferometer has a refractive index of 1.516 while the fibre refractive index is 1.5154 for the core and 1.5161 for the skin.

The theoretical quadratic model is drawn using eq. (5) and plotted as shown in figures 2 and 3. Theoretical imaging of multiple beam interference modulated by step index fibre

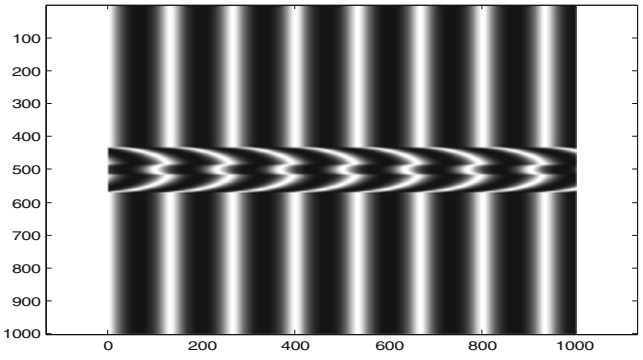

Figure 3. Theoretical imaging of multiple beam interference modulated by step index fibre of fibre radius equal to four times the core radius. The image has matrix dimensions 1024 × 1024 pixels. The fibre diameter has 128 pixels while the core diameter has 32 pixels.

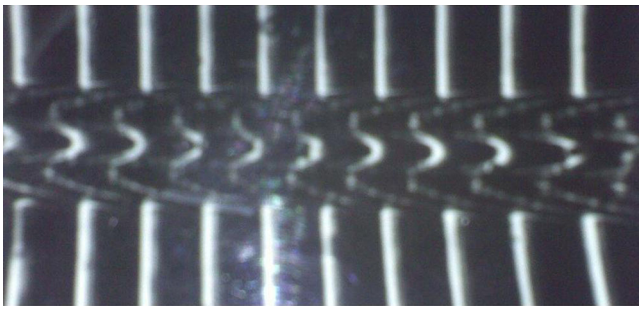

Figure 4. Experimental photograph of straight line fringes modulated by the shift introduced by the cladded glass fibre. The total fibre diameter $t_f = 201.21$ μm. The refractive index of the skin = 1.5154, the refractive index of the core = 1.5161 and the refractive index of the liquid = 1.516. The wavelength of He–Ne laser = 6328 μm. The differential fringe shift of the core = 0.1931. The experiment was carried out at room temperature $T = 32°$C.

of fibre radius equal two times the core radius is shown. The image in figure 2 has matrix dimensions 1024 × 1024 pixels, the fibre diameter has 128 pixels while the core diameter has 64 pixels. In figure 3, a theoretical imaging of multiple beam interference modulated by step index fibre of fibre radius four times the core radius is shown. Also, the image has

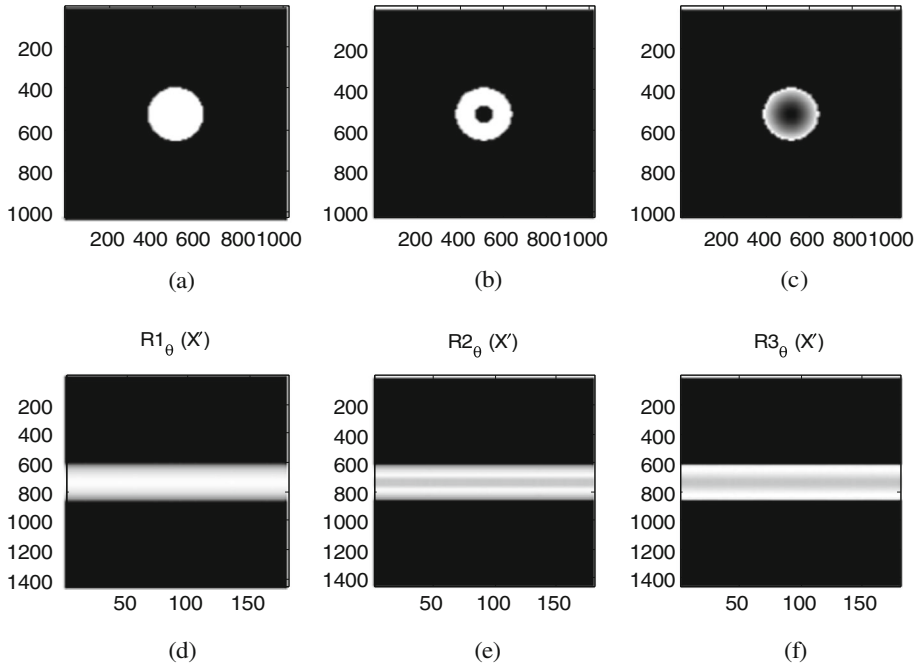

Figure 5. A uniform circular cross-sectional view of (**a**) unclad fibre, (**b**) step index fibre, (**c**) graded index fibre. The corresponding tomographic images are shown in (**d**), (**e**) and (**f**).

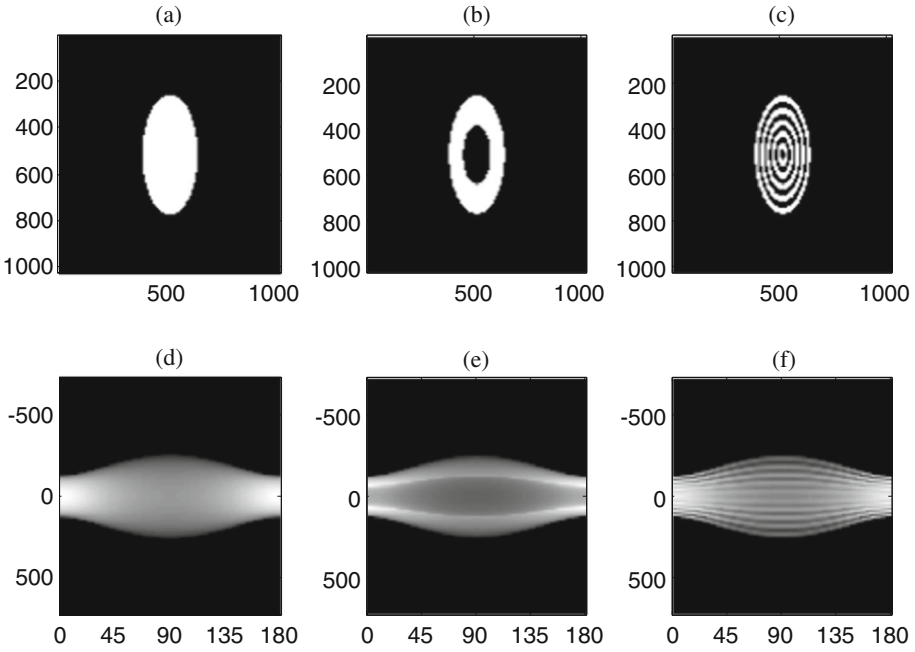

Figure 6. An elliptic deformation from the uniform circular cross-sectional view of (**a**) unclad fibre, (**b**) step index fibre, (**c**) multistep index fibre. The corresponding tomographic images are shown in (**d**), (**e**) and (**f**).

matrix dimensions 102 × 1024 pixels, the fibre diameter has 128 pixels while the core diameter has 32 pixels.

The experimental photograph of the fringe shift occurred due to the cladded fibre in multiple beam interference is shown in figure 4. The total fibre diameter is t_f = 201.21 μm. The refractive index of the skin = 1.5154, the refractive index of the core = 1.5161, and the refractive index of the liquid = 1.516. The wavelength of He–Ne laser = 632.8 nm. The differential fringe shift of the core = 0.1931. The experiment was carried out at room temperature at T = 32°C. The theoretical model of the fringe shift of the clad fibre as in figures 2 and 3 showed a good agreement with the experimental fringe shift for the cladded glass fibre as in figure 4.

The tomographic images of the different circular cross-sections of unclad, step index and graded index fibres are plotted in figure 5. The tomographic image of the unclad fibre resembles a solid cylinder while the step index fibre and graded index fibre resemble a cylinder of graded illumination. The elliptic deformation from the uniform circular cross-section is illustrated in figure 6. The elliptic deformation of fibre cross-section is recognized from the obtained tomographic images. Also, the number of layers present in the graded index fibres is shown referring to the corresponding tomographic image. Also, the tomographic cylinder shows a gross diameter related to the major axis of the ellipse compared to the small width at the ends of the cylinder indicating the minor axis of the cylinder.

4. Conclusion

A theoretical quadratic model proposed for the cladded fibres shows an agreement with the experimental fringe shift obtained in multiple beam interference. The tomographic images corresponding to the cross-sections of fibres leads to recognition of elliptic deformation as well as the number of layers in graded index fibres.

References

[1] S Tolansky, *Surface microtopography* (Longmans Green, London, 1960)
[2] N Barakat and S Mokhtar, *J. Opt. Soc. Am.* **53**, 159 (1963)
[3] N Barakat and A M Hindelah, *Textile Res. J.* **41**, 581 (1964)
[4] N Barakat, *Textile Res. J.* **41**, 167 (1971)
[5] A M Hamed, *Some applications of scattered light and multiple beam interference using coherent light*, M.Sc. Thesis, 1976
[6] N Barakat and A Hamza, *Interferometry of fibrous materials* (Bristol, Adam Hilger, Ltd. Techno House, 1990)
[7] M M El Nicklawy and I M Fouda, *Textile Res. J.* **71**, 252 (1980)
[8] A Hamza, T Z N Sokkar and M A Abeel, *J. Phys. D* **18**, 1773 (1985)
[9] A Hamza, T Z N Sokkar and M A Abeel, *J. Phys. D* **19**, 119 (1986)
[10] N Barakat, A Hamza and A Goned, *Appl. Opt.* **24**, 4383 (1985)
[11] L M Boggs, H M Presby and D Marcuse, *Bell System Tech. J.* **58**, 867 (1979)
[12] H M Presby, D Marcuse, H W Astle and L M Boggs, *Bell System Tech. J.* **58**, 883 (1979)
[13] A M Hamed, *Opt. Appl.* **xxvii**, 229 (1997)
[14] A M Hamed, *Pramana – J. Phys.* **70**, 643 (2008)
[15] R Koprowski and Z Wróbel, *Image processing in optical coherence tomography using Mat-lab* (Univ Silesia, Poland, 2011)
[16] R Gonzalez and R Woods, *Digital image processing* (Addison-Wesley Publishing Company Inc., Boston, MA, USA, 1992)
[17] M Akiba, K P Chan and N Tanno, *Opt. Lett.* **28**, 816 (2003)
[18] D C Adler, T H Ko and J G Fujimoto, *Opt. Lett.* **29**, 2878 (2004)
[19] K Vandersteen, B Busselen, K Van Den Abeele and J Carmeliet, *Geological Society Special Publication* **215**, 61 (2003)
[20] S S Kou and J R C Sheppard, *Appl. Opt.* **48**, 168 (2009)